



IRWIN AND JOAN JACOBS
CENTER FOR COMMUNICATION AND INFORMATION TECHNOLOGIES

On the Role of Exponential Functions in Image Interpolation

Hagai Kirshner and Moshe Porat

CCIT Report #683
January 2008

 Electronics
Computers
Communications

DEPARTMENT OF ELECTRICAL ENGINEERING
TECHNION - ISRAEL INSTITUTE OF TECHNOLOGY, HAIFA 32000, ISRAEL



On the Role of Exponential Functions in Image Interpolation

Hagai Kirshner and Moshe Porat

Department of Electrical Engineering, Technion–Israel Institute of Technology
Haifa 32000, Israel
kirshner@tx.technion.ac.il, mp@ee.technion.ac.il

Abstract

A reproducing-kernel Hilbert space approach to image interpolation is introduced. In particular, the reproducing kernels of Sobolev spaces are shown to be exponential functions. These functions, in turn, give rise to alternative interpolation kernels that outperform presently available designs. Both theoretical and experimental results are presented.

I. INTRODUCTION

Interpolation is needed in image processing tasks such as rotation, translation, resizing and derivative evaluation. The underlying idea in current interpolation methods corresponds to regularity constraints imposed on the continuous-domain image where the pixel values provide its sampled version. For example, sinc-based interpolation kernels assume bandlimitedness (apodized sinc, discrete sinc [1]) while other methods assume piecewise polynomial models (nearest neighbor, linear, Schaum, Keys, Dodgson, B-spline, Meijering and OMOMS [2]). Every model converges to the original function as the sampling interval shortens and the corresponding approximation error can be characterized by [3]:

$$\|\mathbf{x} - \hat{\mathbf{x}}\|_{L_2} \propto C \cdot \Delta^L \cdot \|\mathbf{x}^{(L)}\|_{L_2}. \quad (1)$$

Here, \mathbf{x} is the original continuous domain signal, $\mathbf{x}^{(L)}$ is its L th derivative, $\hat{\mathbf{x}}$ is the interpolated signal and Δ is the sampling interval. In such a formulation, the parameters L and C are the approximation order and the proportional constant, respectively; they provide a means for comparing the various reconstruction (interpolation) methods. Both theoretical and experimental studies have shown that B-spline interpolation kernels perform better in this regard [2], [4], [5].

In spite of the power-law convergence of the approximation error to zero, current interpolation kernels do not necessarily provide the best possible continuous domain model for the whole set of finite-energy functions and a less restrictive regularization constraint other than the piecewise polynomial or bandlimited functions may be considered in this regard. It is suggested here to use the Sobolev space framework for this purpose instead.

Sobolev spaces consist of smooth functions and they serve as the underlying continuous-domain model in several image processing algorithms [6]–[9]. Nevertheless, it seems that the reproducing-kernel Hilbert space (RKHS) property of these spaces has not been investigated within the context of image interpolation; Sobolev functions are dense in L_2 and the suggested approach may further reduce the approximation error of (1). It will be shown that the reproducing kernels of certain Sobolev spaces correspond to exponentials that give rise to interpolating functions. These functions will be then shown to have attractive properties in terms of approximation error characterization while experimental results will be further shown to support these findings.

II. REPRODUCING KERNELS OF SOBOLEV SPACES

Let H_2^p be the Sobolev space of order p . This space consists of all one-dimensional finite-energy functions defined on the real line for which their first p derivatives are of finite energy as well [10]. The corresponding inner product is given by

$$\langle \mathbf{x}, \mathbf{y} \rangle_{H_2^p} = \sum_{n=0}^p \lambda_n \cdot \langle \mathbf{x}^{(n)}, \mathbf{y}^{(n)} \rangle_{L_2}, \quad (2)$$

where $\{\lambda_n\}$ is an arbitrary set of positive numbers and

$$\langle \mathbf{x}, \mathbf{y} \rangle_{L_2} = \int_{-\infty}^{\infty} \mathbf{x}(s) \cdot \overline{\mathbf{y}(s)} ds. \quad (3)$$

It then follows that the reproducing kernel of H_2^p is given by

$$\varphi(s, t) = \mathcal{F}^{-1} \left\{ \frac{1}{\lambda_0 + \lambda_1 \omega^2 + \dots + \lambda_p \omega^{2p}} \right\} (s - t), \quad (4)$$

where \mathcal{F}^{-1} denotes the inverse Fourier transform operation. Recalling the binomial coefficients, one may choose $\lambda_n = \binom{p}{n}$ to yield

$$\varphi(s, t) = \mathcal{F}^{-1} \left\{ \frac{1}{(1 + \omega^2)^p} \right\} (s - t) \quad (5)$$

and the ensued kernels correspond to exponential functions as given in Table I. Other choices for $\{\lambda_n\}_n$ will not be considered here. Being an RKHS, the Sobolev space framework suggests an orthogonal projection interpretation for the ideal sampling process [11], [12]. Let $\mathbf{x}(t)$ be an arbitrary Sobolev function and let $\Lambda = \{t_n\}_n$ be a set of sampling points. It then follows that the sample values satisfy $\mathbf{x}(t_n) = \langle \mathbf{x}(\cdot), \varphi(\cdot, t_n) \rangle_{H_2^p}$ and the set of functions $\{\varphi(\cdot, t_n)\}_n$ constitutes a Riesz basis for their span

$$\mathcal{S} = \overline{\text{Span}} \{ \varphi(\cdot, t_n) \}. \quad (6)$$

The corresponding Gram matrix is given by

$$G(m, n) = \varphi(t_m, t_n), \quad (7)$$

and the orthogonal projection of \mathbf{x} onto the sampling space is given by

$$P_{\mathcal{S}} \mathbf{x} = \sum_n a_n \cdot \varphi(\cdot, t_n). \quad (8)$$

Here, $a = G^{-1}c$ while c denotes the ideal samples of \mathbf{x} on Λ . The unknown portion of \mathbf{x} that is not captured by the sampling process is $P_{\mathcal{S}^\perp} \mathbf{x} = \mathbf{x} - P_{\mathcal{S}} \mathbf{x}$. In shift-invariant cases, where Λ consists of an infinite number of uniformly-spaced sampling points, G^{-1} can be replaced by a proper digital filter; this filter has a rational transfer function originating from the exponential terms composing $\varphi(s, t)$. Table II describes several such filters for a unit sampling step.

TABLE I
REPRODUCING KERNELS OF SOBOLEV SPACES.

Sobolev order, p	$\varphi(s, t)$
1	$\frac{1}{2} e^{- s-t }$
2	$\frac{1}{4} e^{- s-t } \cdot [1 + s-t]$
3	$\frac{1}{16} e^{- s-t } \cdot [3 + 3 s-t + s-t ^2]$
4	$\frac{1}{96} e^{- s-t } \cdot [15 + 15 s-t + 6 s-t ^2 + s-t ^3]$
5	$\frac{1}{768} e^{- s-t } \cdot [105 + 105 s-t + 45 s-t ^2 + 10 s-t ^3 + s-t ^4]$
6	$\frac{1}{7680} e^{- s-t } \cdot [945 + 945 s-t + 420 s-t ^2 + 105 s-t ^3 + 15 s-t ^4 + s-t ^5]$
7	$\frac{1}{92160} e^{- s-t } \cdot [10395 + 10395 s-t + 4725 s-t ^2 + 1260 s-t ^3 + 210 s-t ^4 + \dots$ $\dots + 21 s-t ^5 + s-t ^6]$

TABLE II
DIGITAL FILTERS FOR EXTRACTING REPRESENTATION COEFFICIENTS FROM SAMPLED DATA.

Sobolev order, p	$G(Z)$
1	$2.31304 \cdot (1 - e^{-1}Z^{-1}) \cdot (1 - e^{-1}Z)$
2	$168.044 \cdot \frac{(1 - e^{-1}Z^{-1})^2 \cdot (1 - e^{-1}Z)^2}{(1 + 4.18321Z^{-1}) \cdot (1 + 4.18321Z)}$
3	$321.3686 \cdot \frac{(1 - e^{-1}Z^{-1})^3 \cdot (1 - e^{-1}Z)^3}{3(e^6 - 1) + 8e(Z^{-1} + Z) + 18e^3(Z^{-1} + Z) - 2e^5(Z^{-1} + Z) + e^4(Z^{-2} - 15 + Z^2) - 7e^2(Z^{-2} + 3 + Z^2)}$

III. EXPONENTIAL-BASED INTERPOLATING FUNCTIONS

The sample sequence c , on the other hand, may now be interpreted by means of the representation coefficients of $P_S \mathbf{x}$ with respect to the bi-orthogonal set of $\{\varphi(\cdot, t_n)\}_n$. That is,

$$P_S \mathbf{x} = \sum_n c_n \cdot \psi_n(s), \quad (9)$$

where bi-orthogonality is taken in the Sobolev sense. i.e.,

$$\psi_n(s) = \sum_m G_{n,m}^{-1} \cdot \varphi(s, t_m). \quad (10)$$

Each function ψ_n is composed of a weighted sum of shifted exponential functions and owing to the RKHS property of H_2^p they are interpolant. Figure 1 compares these exponential-based interpolating functions with the B-spline interpolants and with the sinc function. Unlike currently available interpolants, the proposed functions do not comply with the partition-of-unity condition given by

$$1 = \sum_{n=-\infty}^{\infty} \psi(t - n) \quad \forall t \in \mathbb{R}, \quad (11)$$

although the infinite sum on the right-hand-side of the equation does converge to unity as the Sobolev order increases.

When scaling the sampling grid, the ensued interpolating functions $\{\psi_n\}_n$ are scaled accordingly. This scaling property does not apply, however, to the exponential functions $\{\varphi_n\}_n$, which remain unscaled but align themselves to the new sampling grid instead. Nevertheless, both $\{\varphi_n\}_n$ and $\{\psi_n\}_n$ span the same sampling space \mathcal{S} . In this regard, the error kernel introduced in [13] for the shift-invariant case provides a means for comparing between various generating functions (interpolant and non-interpolant). It describes the average L_2 error between the original function and its interpolated version where averaging is taken over all possible phase shifts of the sampling grid. This kernel is given by

$$E(\omega) = \frac{|\sum_{k \neq 0} \Phi(\omega + 2\pi k)|^2 + \sum_{k \neq 0} |\Phi(\omega + 2\pi k)|^2}{|\sum_{k=-\infty}^{\infty} \Phi(\omega + 2\pi k)|^2}, \quad (12)$$

where Φ denotes the Fourier transform of φ . Figure 2 depicts this kernel for several generating functions and it is shown that the proposed exponential functions introduce less approximation error than the B-spline and the OMOMS functions at the required lower frequency band. Unlike other interpolants, however, $E(\omega)$ of the proposed exponential functions does not equal zero at the origin although it converges to this value as p increases.

Following [14], an L_2 orthogonal projection approach is adopted for image scaling. Let c be the ideal samples of $\mathbf{x} \in H_2^p$ taken over a uniform sampling grid of a unit sampling step $\Lambda = \{t_n = n\}_n$; in such a case, one can determine the continuous-domain signal $P_S \mathbf{x}$. Upon scaling, this signal would be projected onto the space \mathcal{S}_Δ , where Δ is the scaling factor, $\mathcal{S} = \overline{\text{Span}}\{\psi_n(s - n)\}_n$ and $\mathcal{S}_\Delta = \overline{\text{Span}}\{\psi_n(s/\Delta - n)\}_n$. The ideal samples of the scaled signal are then given by

$$c_\Delta = A^{-1} \cdot B^{-1} \cdot C^{-1} \cdot D^{-1} \cdot c, \quad (13)$$

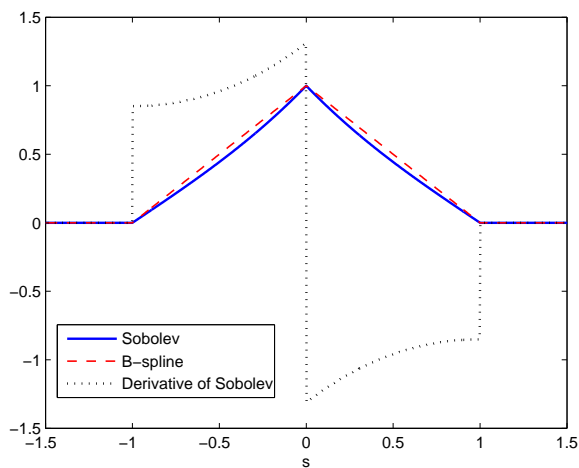
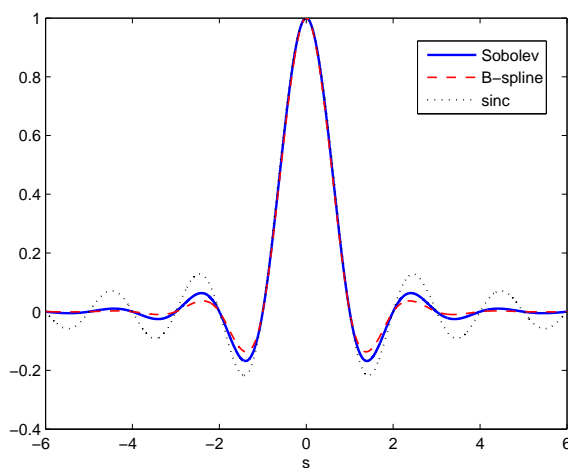
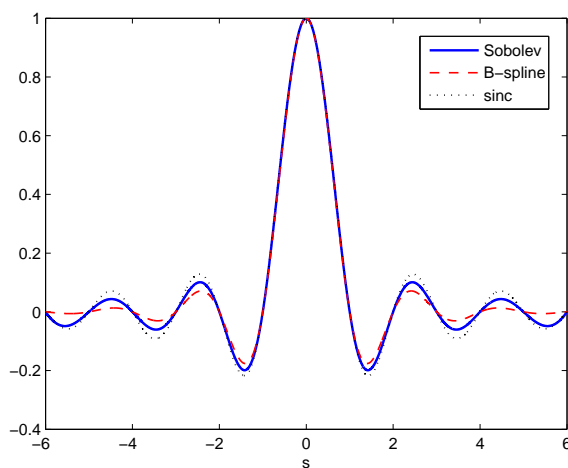
(a) $p = 1$.(b) $p = 3$.(c) $p = 5$.

Fig. 1. Sobolev (solid), B-spline (dashed) and sinc (dotted) interpolants for a unit sampling step. p denotes both Sobolev and B-spline orders.

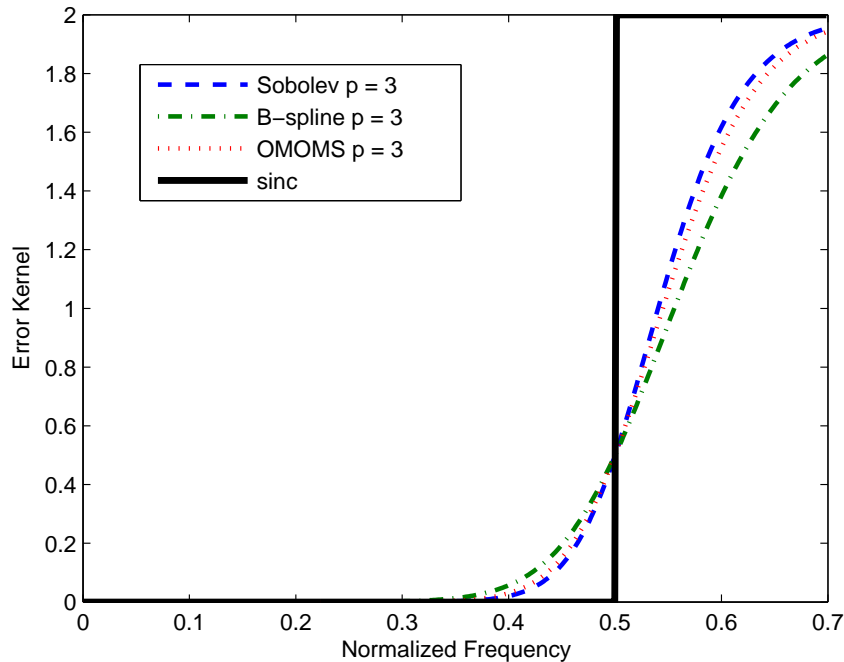


Fig. 2. Error kernel for Sobolev (dashed), for B-spline (dash-dotted), for OMOMS (dotted) and for the sinc (solid) functions. $p = 3$ denotes both the Sobolev and the B-spline orders.

where A, B, C, D are all Gram matrices given by

$$\begin{aligned}
 A_{m,n} &= \phi(\Delta m, \Delta n) & \phi &\in H_2^{2p}, \\
 B_{m,n} &= \phi(\Delta m, \Delta n) & \phi &\in H_2^p, \\
 C_{m,n} &= \phi(m, \Delta n) & \phi &\in H_2^{2p}, \\
 D_{m,n} &= \phi(m, n) & \phi &\in H_2^p.
 \end{aligned} \tag{14}$$

The matrix D^{-1} extracts the representation coefficients of $P_{\mathcal{S}\mathbf{x}}$ with respect to the exponential functions $\{\phi(s, t_n)\}_n$. The matrix C^{-1} extracts the representation coefficients of the L_2 orthogonal projection of $P_{\mathcal{S}\mathbf{x}}$ onto \mathcal{S}_{Δ} . These coefficients correspond to the biorthogonal set of $\{\phi(s, \Delta \cdot t_n)\}_n$ in the L_2 sense, which are not interpolant functions. The matrix B^{-1} extracts the representation coefficients corresponding to $\{\phi(s, \Delta \cdot t_n)\}_n$ and the matrix A^{-1} extracts the representation coefficients of the scaled interpolant functions $\{\psi(s/\Delta - n)\}_n$. This Gram matrix formulation is preferable over the shift-invariant structure due to the finite (rather than infinite) number of samples that are available for an image and it introduces a negligible computational overhead for images of standard size. Nevertheless, the significant values of these Gram matrices are located near the main diagonal and large images may be interpolated by considering a relatively small neighborhood of pixels for every interpolated value. A neighborhood of 15×15 pixels are sufficient in practice for a Sobolev order of $p = 3$. Additionally, both the matrix C and the sampling function of [14] have a similar role in scaling an image by means of an orthogonal projection. Nevertheless, the values of C are explicitly given here and no Gaussian approximation is required in this regard.

A separable model is suggested in this work although the reproducing kernel of a two-dimensional Sobolev space is not a separable function; the Fourier transform of such kernels is given by $\Phi(u, v) = 1/(1 + u^2 + v^2)^p$, $p \geq 2$ and the radially symmetric space-domain kernels are given by $\phi(r) = 2\pi^p r^{p-1} K_{p-1}(2\pi r)/\Gamma(p)$, where $r^2 = x^2 + y^2$, $K_n(\cdot)$ denotes the Bessel function of the third kind of order n , and Γ is the gamma function. Nevertheless, a separable model allows for a relatively short run-time implementation that is comparable with the separable model of the B-splines functions.

IV. EXPERIMENTAL RESULTS

The proposed exponential kernels have been compared with the cubic B-spline interpolation function while considering a Sobolev order of $p = 3$. Two separate operations have been examined: rotation and scaling, and the Gram matrix formulation was implemented for both methods. Such an implementation for the B-spline approach was shown to yield better SNR values of more than 2[dB] over digitally filtering the samples as suggested by [2]. Also, the Gram matrix formulation does not require extracting the image by its mirror version as needed in the shift-invariant case.

Following [15], successive image rotations have been applied to a given image until it reached its starting position allowing for an SNR calculation. Figure 3 depicts several such rotations of an image using the proposed interpolating functions. Additional results are given in Table III suggesting that these functions outperform the B-splines functions. SNR values have been calculated based on the circular region shown on the bottom-right image of Figure 3 having a diameter of 90 percent of the image's dimension.

Nevertheless, when considering larger circular areas, boundary effects lead to more prominent results in favor of the proposed interpolating functions. Figure 4 depicts a detailed view of the rectangular area shown on the bottom-right image of Figure 3. It is evident that while B-spline interpolants introduce boundary effects, the proposed functions do not. This property was also observed in the scaling experiment. An additional comparison is given in Figures 5 - 7 showing final images of the rotation experiment; one can observe that the proposed functions perform better visually as well.

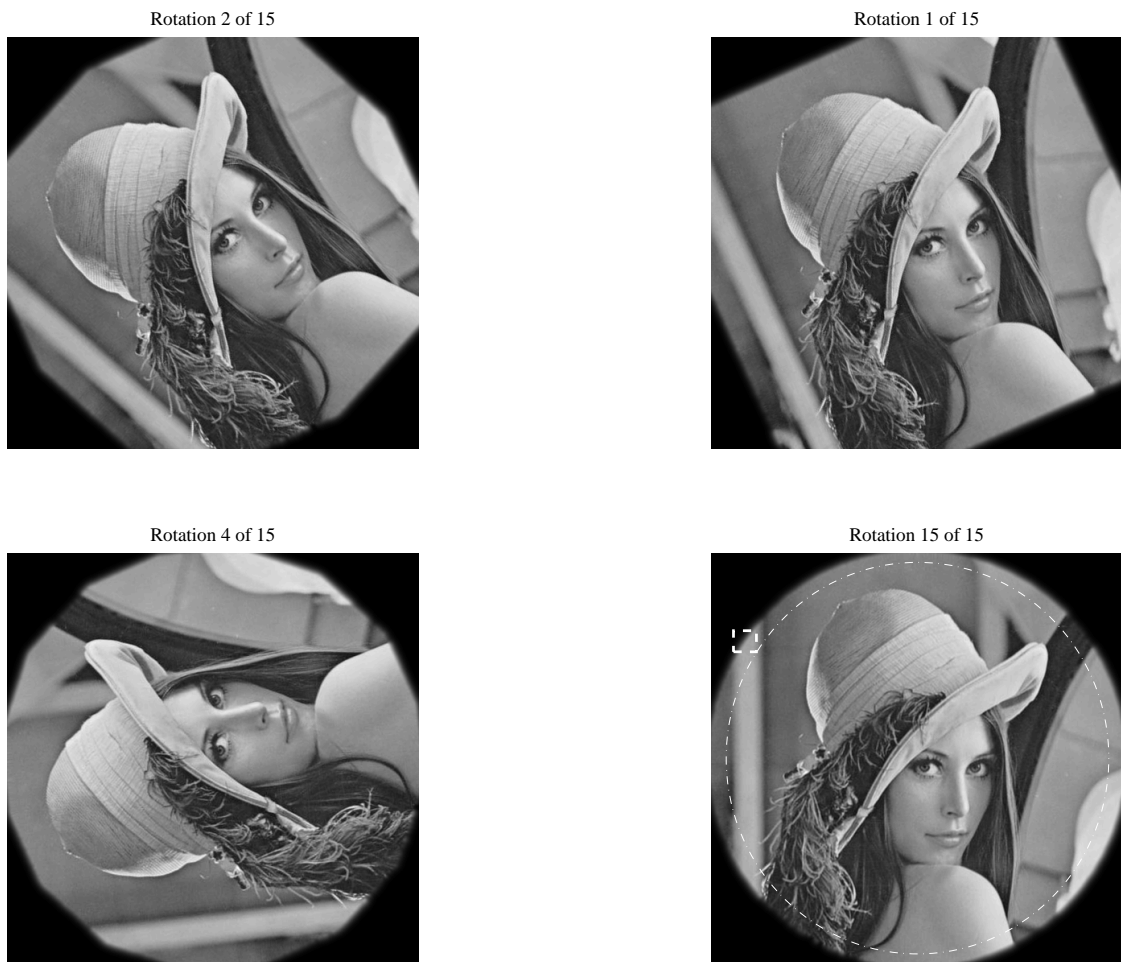
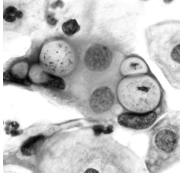


Fig. 3. Rotation of an image using the proposed exponential-based interpolants.

The image scaling experiment involves two consecutive reciprocal resizing operations [14] so the doubly scaled image can be compared with the original one. As for an enlargement followed by a reduction, high SNR values

TABLE III
A COMPARISON OF IMAGE ROTATION

Image		SNR [dB]			
		15 Rotations		100 Rotations	
		B-spline	Sobolev	B-spline	Sobolev
	Brain MRI	32.2	33.7	28.2	30.5
	Pap smear	47.0	48.6	43.7	47.1
	Lena	32.0/33.9/34.29 ^a	36.0	26.9	30.1
	Fishing Boat	30.4/31.2/33.8 ^a	33.4	26.8	29.0
	Pepper	30.8	31.8	28.2	29.7
	Bridge	24.5	25.8	21.2	22.9

^aThe three values correspond to B-spline interpolation by digital filtering [2], [16]; to cubic B-spline interpolation by Gram matrix computation as implemented in this work; and to cubic OMOMS interpolation [16].

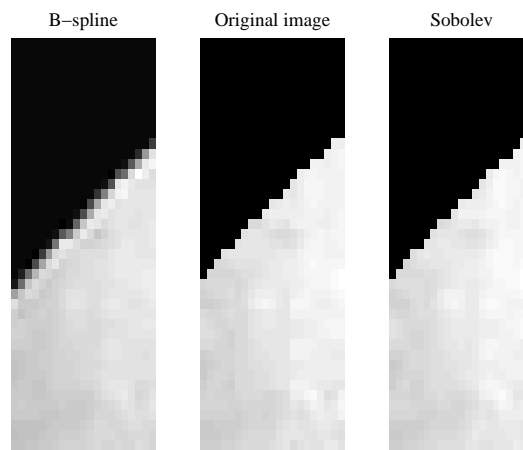
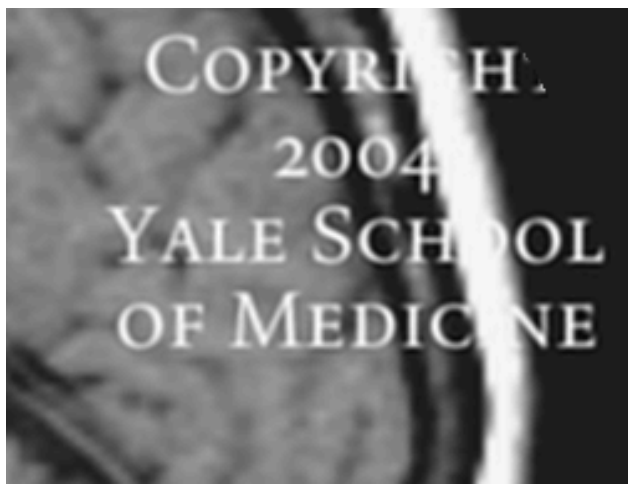
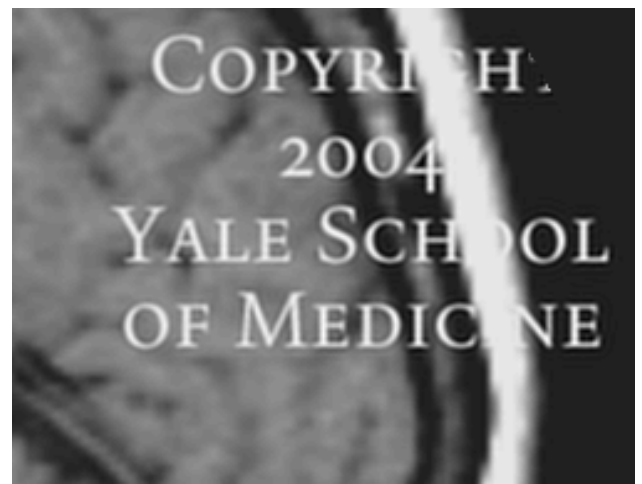


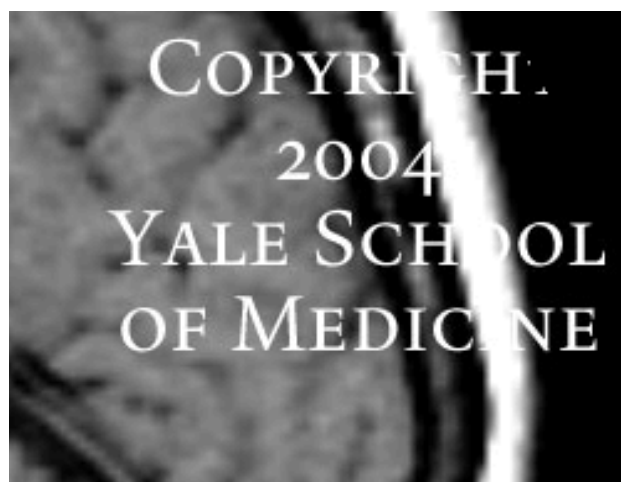
Fig. 4. An image boundary. Shown is the rectangular area of Figure 3. Further image details are shown in Figs 5-7.



(a) B-spline. SNR = 28.2[dB].



(b) Sobolev. SNR = 30.5 [dB].



(c) Original.

Fig. 5. A comparison of an image rotation having applied 100 rotations of 3.6° each. Shown is a portion of the Brain MRI image while SNR values are given for the full image.



(a) B-spline. SNR = 26.9[dB].



(b) Sobolev. SNR = 30.1[dB].



(c) Original.

Fig. 6. Similar to Figure 5. Shown is a portion of the image of Lena.

of more than 60[dB] were reported for the cubic B-spline interpolants [14] and similar values are achieved by the proposed exponential functions. Therefore, such cases will not be presented here. Figure 8 depicts an example of scaling and of unscaling an image by a factor of $\sqrt{18}$ using the proposed exponential-based interpolation functions. Figure 9(a) compares the proposed interpolants with the B-spline interpolants for several scaling factors while excluding a boundary frame of five pixels on each side of the image. Similar to the rotation experiment, more prominent results are reported when including the boundary pixels in the SNR calculations as shown in Figure 9(b). Investigation of other images yields similar results. It is noted that the B-spline implementation of the scaling experiment provides exact evaluation of the 'sampling function' of [14] (using the Spline toolbox of Matlab) rather than using the Gaussian approximation scheme suggested there.



(a) B-spline. SNR = 24.3[dB].



(b) Sobolev. SNR = 26.3[dB].



(c) Original.

Fig. 7. Similar to Figure 5. Shown is a portion of the Fishing Boat image.

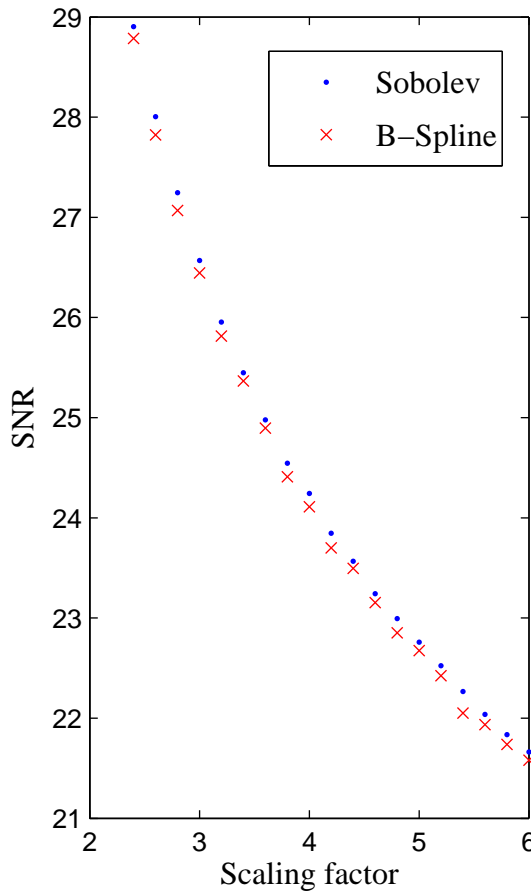


(a)

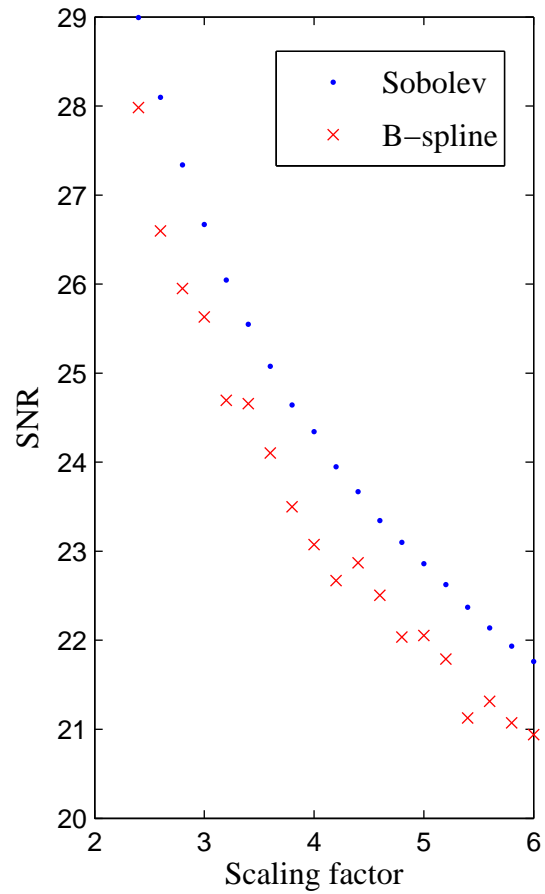


(b)

Fig. 8. Image scaling by a factor of $\sqrt{18}$. Shown are the scaled version (a) and the unscaled version (b) of the image of Lena.



(a)



(b)

Fig. 9. A comparison of scaling performance for the image of Lena. (a) SNR values while excluding the boundaries of the image. (b) SNR values while including the boundaries (b).

V. CONCLUSIONS

A new approach to image interpolation based on a reproducing-kernel Hilbert space approach has been proposed. Sobolev smooth functions are dense in L_2 and the Sobolev space framework is very useful for this purpose. The reproducing kernels of these spaces are shown to be exponential functions and the ideal sampling process is characterized by a set of proper inner products. These kernels also give rise to interpolation functions that outperform currently available interpolation methods. Both theoretical and experimental results have been presented involving rotation and scaling of an image. Our conclusion is that the new method of image interpolation could be a helpful alternative to the use of B-spline in interpolation tasks.

ACKNOWLEDGMENTS

This work was supported in part by a grant from the GIF, the German-Israeli Foundation for Scientific Research and Development, by the Eshkol Fund of the Israeli Ministry of Science, and by the Ollendorff Minerva Centre. Minerva is funded through the BMBF.

REFERENCES

- [1] L. P. Yaroslavsky, "Efficient algorithm for discrete sinc-interpolation," *Applied Optics*, vol. 36, no. 2, pp. 460–463, January 1997.
- [2] P. Thévenaz, T. Blu, and M. Unser, "Interpolation revisited," *IEEE Trans. Medical Imaging*, vol. 19, pp. 739–758, July 2000.
- [3] M. Unser and I. Daubechies, "On the approximation power of convolution-based least squares versus interpolation," *IEEE Trans. Signal Processing*, vol. 45, no. 7, pp. 1697–1711, July 1997.
- [4] T. M. Lehmann, C. Gönner, and K. Spitzer, "Survey: Interpolation methods in medical image processing," *IEEE Trans. Medical Imaging*, vol. 18, pp. 1049–1075, November 1999.
- [5] E. H. W. Meijering, W. J. Niessen, and M. A. Viergever, "Quantitative evaluation of convolution-based methods for medical image interpolation," *Med. Image Anal.*, vol. 5, no. 2, pp. 111–126, 2001.
- [6] D. Mumford and J. Shah, "Optimal approximations by piecewise smooth functions and associated variational problems," *Comm. Pure Applied. Math.*, vol. 42, pp. 577–685, 1989.
- [7] T. F. Chan and J. Shen, *Image Processing And Analysis: Variational, PDE, Wavelet, And Stochastic Methods*. SIAM, 2005.
- [8] B. Burgeth, S. Didas, and J. Weickert, "The Bessel scale-space," in *Deep Structure, Singularities, and Computer Vision*, O. F. Olsen, L. Florack, and A. Kuijper, Eds. Berlin: Springer, 2005, pp. 84–95.
- [9] H. Kirshner and M. Porat, "On interpolation of differentially structured images," in *EUSIPCO*, 2007.
- [10] R. A. Adams, *Sobolev spaces*. New York, NY: Academic Press, 1975.
- [11] H. Kirshner and M. Porat, "On the approximation of L_2 inner products from sampled data," *IEEE Trans. Signal Processing*, vol. 55, no. 5, pp. 2136–2144, May 2007.
- [12] T. G. Dvorkind, H. Kirshner, Y. C. Eldar, and M. Porat, "Minimax approximation of representation coefficients from generalized samples," *IEEE Trans. Signal Processing*, vol. 55, no. 9, pp. 4430–4443, September 2007.
- [13] T. Blu and M. Unser, "Quantitative Fourier analysis of approximation techniques: Part I - Interpolators and projectors," *IEEE Trans. Signal Processing*, vol. 47, no. 10, pp. 2783–2795, October 1999.
- [14] M. Unser, A. Aldroubi, and M. Eden, "Enlargement or reduction of digital images with minimum loss of information," *IEEE Trans. Image Processing*, vol. 4, no. 3, pp. 247–258, March 1995.
- [15] M. Unser, P. Thévenaz, and L. Yaroslavski, "Convolution-based interpolation for fast, high-quality rotation of images," *IEEE Trans. Image Processing*, vol. 4, pp. 1371–1381, October 1995.
- [16] T. Blu, P. Thévenaz, and M. Unser, "Moms: Maximal-order interpolation of minimal support," *IEEE Trans. Image Processing*, vol. 10, pp. 1069–1080, July 2001.